The Source of Helicity in Perfluorinated *N*-Alkanes

Seung Soon Jang, Mario Blanco, and William A. Goddard III

Materials and Process Simulation Center, Beckman Institute, California Institute of Technology, Pasadena, California 91125

Gregg Caldwell and Richard B. Ross

Advanced Materials Technology Center, 201-2E-23, 3M Company, St. Paul, Minnesota 55144

Received September 5, 2002; Revised Manuscript Received April 29, 2003

ABSTRACT: The well-known helical conformations of double stranded DNA and poly(alanine) are stabilized by inter- and intramolecular hydrogen bonds, respectively. Perfluorinated *n*-alkanes also exhibit stable helical conformations, with ordered chiralities at low temperatures. In the absence of hydrogen bonds, one may ask what forces stabilize perfluorinated *n*-alkane helices. We combine ab initio and empirical data to study the likely classical source of this helical behavior. Past studies point to bad sterics (van der Waals interactions) between neighboring fluorine atoms as the source of helicity in perfluorinated linear alkanes. In these early studies electrostatics were ignored. We undertook a detailed force field parameter optimization strategy, using experimental and ab initio data, to obtain transferable, uncorrelated estimates of the separate classical energy components. We find that the dominant energy term, the source of helicity, is electrostatics. The coulomb repulsion, from a classical fixed-charge model, reproduces reasonably well the position of the energy minima and the energy barrier between the helical and the all-trans conformations. Polarization effects, changes in atomic charges as a result of conformational changes, are not significant. Dihedral interactions and van der Waals terms adjust the exact position of the minima only slightly. In the absence of electrostatic contributions, van der Waals and dihedral interactions predict the incorrect stable conformations.

1. Introduction

X-ray crystallography experiments[1] conducted nearly 50 years ago indicate the appearance at room temperature of a partly disordered crystalline phase for poly-(tetrafluoroethylene) (PTFE). This transformation (ca. 20 °C) occurs significantly below the 327 °C melting point. The phase transition is believed to be a transformation from well-ordered helical chains to more disordered polymer conformations. More recently, IR measurements have confirmed the existence of multiple minima on the perfluorinated backbone.[2] It is important to understand the origin of such multiple conformations in linear perfluorinated compounds not only because these conformations influence mechanical, rheological, and surface properties at room temperature but also because our ability to break down fundamental quantum energies into classical interaction potentials is greatly challenged by these compounds.

Various force fields for fluorinated compounds have been developed, some include the effect of polarizability in conformational energies.[3] The twisted nature of perfluorinated *n*-alkanes has been attributed to repulsive van der Waals interactions among fluorine atoms[4−6] located at 1−5 positions along the carbon backbone. Presumably the size of these atoms lead to steric repulsions that, compared to the corresponding hydrogen atoms in polyethylene, destabilize the all-trans conformation. In general fluorinated alkanes exhibit a torsional twist on the backbone angles which results in two minima around the standard trans and gauche conformations. Although such conformations can be reproduced with a multicomponent Fourier torsion potential, such an approach obscures the intrinsic origin of the helical conformations. We report both a multicomponent Fourier as well as a simple Dreiding type, single term, torsion potential. Either of the choices yield similar results in regards to the source of helicity.

Because of the number of electrons involved, high-level quantum calculations on perfluorinated hydrocarbons remain a challenge. Nevertheless, Dixon[4] reported a 15.3° twist in the central carbon bond in perfluorinated *n*-butane. Smith et. al,[5] showed that the twist in perfluorobutane (PFB) and perfluoropentane (PFP) can be represented by a six-state rotational isomeric state (RIS) model. More recently[7] a rather extensive study of the low-pressure phase diagram of PTFE has been conducted using molecular dynamics and the 12-6 Lennard-Jones parameters of Nose−Klein[8] with judicious choices for dihedral potentials. For simplicity partial charges were not included in the potential energy expression. This potential failed to predict the helical conformation as the stable form under ambient conditions. In the present work, we propose a new force field which includes electrostatics. For consistency it is essential to refine the rest of the force field parameters, including valence and van der Waals terms. Furthermore, we require that the physical properties of perfluorinated compounds be reproduced with a single set of force field parameters for the solid, liquid, and gas states for a series of linear perfluorinated alkanes. Previous work successfully used a similar procedure in modeling the crystal and amorphous phases of PVDF.[9,10]

Ultimately, the quantum-electronic properties of perfluorinated *n*-alkanes are intrinsically responsible for their observed helical conformations. However, a successful breakdown of the classical energy components affecting the conformational stability of perfluorinated *n*-alkanes may be of great importance in determining properties not accessible through quantum mechanical means (e.g., phase transformations of large unit cells). Thus, to help elucidate the origin of helicity in perfluorinated *n*-alkanes we used a step-by-step procedure to obtain as uncorrelated force field parameters as possible. Thus, in section 2.1, we present DFT B3LYP calculations on gas-phase perfluoromethane to deter-

Table 1. Valence Force Field for CF$_4$

bond stretching	$E_r = \frac{1}{2}K_r(R - R_0)^2$
valence angle bending	$E_\theta = \frac{1}{2}(K_\theta/\sin^2\theta_0)(\cos\theta - \cos\theta_0)^2$
bond-bond cross term	$E_{rr} = K_{rr}(R_1 - R_{1,0})(R_2 - R_{2,0})$
bond-angle cross term	$E_{r\theta} = (\cos\theta - \cos\theta_0)\{(K_{r\theta1}/\sin\theta_1)(R_1 - R_{1,0}) - (K_{r\theta2}/\sin\theta_2)(R_2 - R_{2,0})\}$

E_r	C−F	K_r	944.7	R_0	1.226		
E_θ	F−C−F	K_θ	77.1	θ_0	141.9		
E_{rr}	F−C−F	K_{rr}	128.9	$R_{1,0} = R_{2,0}$	1.226		
$E_{r\theta}$	F−C−F	$K_{r\theta_1} = K_{r\theta_2}$	62.7	$R_{1,0} = R_{2,0}$	1.226	θ_0	141.9

mine a high quality spectroscopic valence force field for CF$_4$. These calculations, together with the experimentally determined X-ray structure,[18] *P−V* diagram, and compressibility curve for CF$_4$,[31,35] were used in section 2.2 to extract reliable, and transferable, van der Waals parameters. Transferability was tested by direct comparison with experimental densities and solubility parameters (heats of vaporization) of C$_2$F$_6$, C$_3$F$_8$, and C$_4$F$_{10}$ (section 2.2). Three schemes for assigning quantum mechanical point charges are presented in section 2.3.

Quantum calculations on perfluorohexane (PFH) were performed to complete the determination of the valence force field. After full geometry optimization, the Hessian matrix of second-order derivatives was calculated and vibrational modes and vibrational frequencies fitted with standard dihedral potentials. These results are presented in sections 2.4 and 3.1. Although a single Fourier term dihedral potential was adequate to fit the vibrational frequencies around the most stable conformation, we also performed quantum calculations, over the full range of dihedral conformations, to obtain a multicomponent dihedral potential adequate for fitting the internal energies and energy barriers between all stable conformers. A detailed breakdown of the energetics near the stable helical conformation is provided in section 3.1. Section 3.2 further validates the current force field for higher perfluorinated *n*-alkanes. Section 4 presents a critical discussion of the origin of helicity.

2. Force Field

We need a clear strategy for the determination of a force field for perfluorinated *n*-alkanes, capable of an unambiguous classical energy separation into individual components. We begin by determining the valence force field for CF$_4$, which requires neither assumptions on the correct nonbond interaction potential nor a dihedral potential. We use the Hessian-biased singular value decomposition (HBSVD) method[13,14] to reproduce the molecular vibrational frequencies, which are essential to evaluate the thermochemical properties of CF$_4$ and the zero point energy correction. Second, on the basis of this predetermined valence force field, the molecular crystal structure of CF$_4$ is iteratively simulated through molecular dynamics methods at various temperature and pressure conditions until the best parameter set fitting to the experimental phase diagram is obtained. Subsequently, the predicted thermodynamic properties, liquid densities, and cohesive energies (heats of vapor-

ization) of low molecular weight perfluoroalkanes are checked to confirm the accuracy of the force field parameters. Prior to the estimation of thermodynamic properties of the higher alkanes, quantum calculations are performed to settle on a scheme for the assignment of atomic charges (section 2.3) and to extract the require dihedral potential (section 2.4). using again the HBSVD method to decompose the Hessian matrix of second-order derivatives of the energy with respect to changes in coordinates for a series of simple perfluorinated *n*-alkanes.

2.1. CF$_4$ Valence Force Field. The HBSVD method utilizes the experimental molecular vibration frequencies[15] as well as a quantum mechanical Hessian matrix of second-order derivatives of the energy with respect to atomic coordinate displacements. We use the 6-31G* basis set and B3LYP exchange-correlation functional from which Mulliken charges are calculated and assigned on CF$_4$: atomic partial charges, in electron units are +0.9505 for carbon and −0.2376 for fluorine. At this point, it is not necessary to consider the van der Waals interaction because 1−2 and 1−3 nonbond interactions in CF$_4$ are completely excluded. The molecular vibrational frequencies based on the valence force field (Table 1) were calculated using the Vibrate module in PolyGraf and compared to the experimental observation as shown in Table 2. The values are in good agreement with experimental results.[15]

2.2. van der Waals Force Field. The van der Waals parameters for fluorine were optimized next. In this paper, the exponential-6 type (X6) function (eq 1) was used to describe the van der Waals interaction potential. The Lennard-Jones 12-6 is simpler (two parameters rather than three) and faster to compute (eliminating a square root and an exponentiation). However our experience is that the X6 form gives a somewhat better description of van der Waals interactions.[16]

$$E_{vdW,ij} = D_{vdW}\left[\left(\frac{6}{\zeta - 6}\right)\exp\left(\zeta\left(1 - \frac{R_{ij}}{R_{vdW}}\right)\right) - \left(\frac{\zeta}{\zeta - 6}\right)\left(\frac{R_{ij}}{R_{vdW}}\right)^{-6}\right] \quad (1)$$

where D_{vdw} is the energy well depth, R_{vdW} is the distance at the energy minimum, and ζ is a dimensionless constant related to the stiffness of the inner repulsive wall. The van der Waals parameters for carbon were not changed from those for carbon in poly(ethylene)[17] and poly(vinylidene fluoride).[9] This makes it possible to simulate a partially fluorinated hydrocarbon compound with the level of accuracy of the Dreiding force field[16] without introducing additional parameters.

For the purpose of optimizing the fluorine van der Waals parameters, we use the experimental molecular crystal structure[18] of tetrafluoromethane (CF$_4$), obtained from high-resolution powder neutron diffraction data at 1.5 K. Additional accurate experimental data, both thermodynamic data and a molecular crystal structure,

Table 2. Molecular Vibrational Frequencies of CF$_4$

		frequencies (cm^{-1})	
symmetry species	type of mode	calculated	experimental[15]
A1	symmetric stretch	909.0	909.1
E	degenerate symmetric bend	435.2, 435.3	435.4
F2	degenerate stretch	1283.6, 1283.6, 1283.6	1283.7
	degenerate symmetric deformation	630.8, 630.8, 630.9	631.1

Table 3. van der Waals Parameters for C and F[a]

	van der Waals parameters of exponential-6			density (g/cm³)[c]	$\Delta_{sub}H$ (kcal/mol)[d]
	ζ	D_{vdW}	R_{vdW}		
C[b]	12	0.084 40	3.8837		
F	12	0.044 53	3.4985	2.2247 ± 0.0475	4.06
	13	0.047 20	3.4480	2.2252 ± 0.0413	4.07
	14	0.049 35	3.4112	2.2244 ± 0.0389	4.06
	15	0.050 92	3.3825	2.2243 ± 0.0360	4.06
	16	0.052 46	3.3589	2.2253 ± 0.0349	4.06

[a] The calculations were carried out for the experimental structure at 1.5 K. [b] The optimum parameters for carbon were fixed in this study at the value obtained from previous studies on fluorocarbons.[9,17] [c] Experimental 2.2249 g/cm³.[18] [d] Experimental 4.06 kcal/mol.[19,20]

are available.[19,20] The experimental structure was compared to *NPT* molecular dynamics simulation results at the same pressure and temperature condition averaged over 50 ps, with an integration time step of 1 fs, using an ensemble consisting of 1280 atoms (a 4 × 4 × 4 expanded cell). Verlet leapfrog integration method[21] and Ewald sums[22] were used in the simulations. The Nose−Hoover[23−26] and the Parrinello−Rahman methods[27−29] were used to control the temperature and pressure, respectively. The enthalpy of sublimation ($\Delta_{sub}H$) at 76 K was used as an independent check for the van der Waals parameter set selection. This was calculated according to eq 2:

$$\Delta_{sub}H = (E_{potential}^{gas} + E_{T=0K}^{gas} + \Delta H_{T=76K}^{gas}) - (E_{potential}^{crystal} + E_{T=0K}^{crystal} + \Delta H_{T=76K}^{crystal})/4 \quad (2)$$

where $E_{potential}$ and $E_{T=0K}$ are potential energy and zero-point-energy for each state, respectively, and $\Delta H_{T=76K}$ for the gas phase is assumed to be ideal. For the crystal state, a 5 × 5 × 5 Brillouin zone was considered to calculate the phonon spectra of the crystal. The pressure−volume work in the solid state was neglected. The experimental value for the enthalpy of sublimation at 76 K was reported as 4.06[19,20] and 4.016 kcal/mol,[30] respectively

In this study, five sets of R_{vdW} and D_{vdW} parameters for fluorine were optimized for five different values of the exponential 6ζ parameter. Each set was able to reproduce the density and enthalpy of sublimation experimentally reported with good agreement as shown in Table 3. Thus, D_{vdW} is in the narrow range from 44 to 52 cal/mol (22.4−26.4 K), while R_{vdW} is restricted to values within 3.36 and 3.49 Å.[8] Details on the final selection of the van der Waals parameters for fluorine are given at the end of this section.

Figure 1 shows the pressure−volume isotherm of the CF_4 crystal obtained through *NPT* MD simulation at 77 K using the parameter sets in Table 3. The values from our MD simulations seem to be systematically offset from the experimental *PV* isotherms, perhaps due to the neglect of zero point energies in the force field, which would yield an increase in the molar volume at low temperatures for all pressures.

An alternate source of this discrepancy may be experimental errors as pointed out by Nose and Klein.[8] This discrepancy may be attributed to the experimental procedure[31] used to get the *PV* isotherm, in which the molar volume is measured at a temperature (77 K) close to the melting temperature of CF_4 (89 K). This effect is more pronounced on the light fluorocarbon compounds. Orientational liquid states (or plastic crystalline phases)
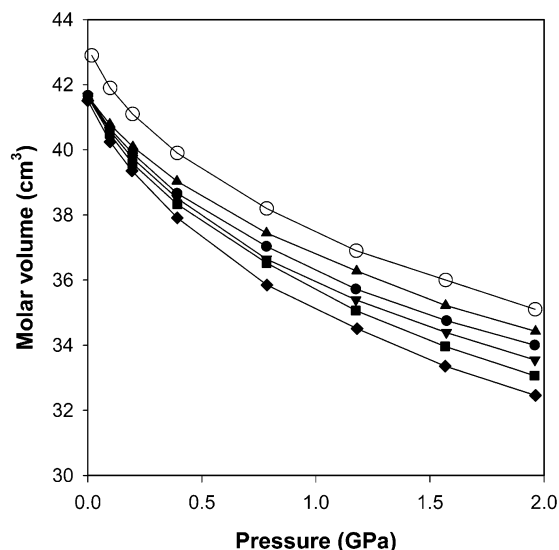

Figure 1. *PV* isotherm of CF_4 crystal at 77 K: ○, experiment (ref 31); ▲, simulation ($\zeta = 16$); ●, simulation ($\zeta = 15$); ▼, simulation ($\zeta = 14$); ■, simulation ($\zeta = 13$); ♦, simulation ($\zeta = 12$).
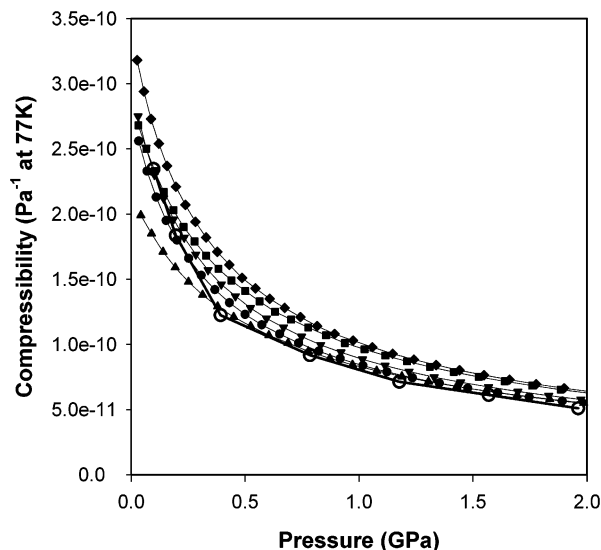

Figure 2. Comparison of compressibilities from simulated *PV* isotherm of CF_4 crystal at 77 K: ○, experiment (ref 31); ▲, simulation ($\zeta = 16$); ●, simulation ($\zeta = 15$); ▼, simulation ($\zeta = 14$); ■, simulation ($\zeta = 13$); ♦, simulation ($\zeta = 12$).

are exhibited by the quasi-globular halomethanes CF_4 and C_2F_6.[32]

The compressibility $\beta = -(1/V)(\partial V/\partial P)_T$ was calculated by differentiating the Murnaghan-Birch's equation of state[33,34] fitted to each simulated *PV* isotherm:

$$P = \frac{3}{2\beta_0}\left[\left(\frac{V_0}{V}\right)^{7/3} - \left(\frac{V_0}{V}\right)^{5/3}\right]\left[1 - \xi\left\{\left(\frac{V_0}{V}\right)^{2/3} - 1\right\}\right] \quad (3)$$

where β_0 and V_0 are compressibility at zero pressure and molar volume at zero pressure, respectively, and ξ is an adjustable constant.

Among the tried parameter sets, the set with $\zeta = 15$ showed the best agreement with the experimental compressibility[31] as shown in Figure 2. The temperature−volume relation was also investigated on the basis of the parameter set with $\zeta = 15$ (Figure 3). Overall, good agreement between the simulation results, using the fluorine parameter set ($D_{vdW} = 0.05092$, $R_{vdW} =$

Table 4. Densities and Solubility Parameters of Small Perfluoroalkane Compounds vs Charge Assignment Method

	C_2F_6		
	ref	Mulliken	ESP
density (g/cm^3)	1.60	1.66 ± 0.03	1.63 ± 0.07
solubility parameters (cal/cm^3)$^{1/2}$	6.33 ± 0.19	6.76 ± 0.22	6.56 ± 0.49
	C_3F_8		
	ref	Mulliken	ESP
density (g/cm^3)	1.61	1.66 ± 0.05	1.61 ± 0.06
solubility parameters (cal/cm^3)$^{1/2}$	6.02 ± 0.60	6.41 ± 0.31	6.24 ± 0.28
	C_4F_{10}		
	ref	Mulliken	ESP
density (g/cm^3)	1.60	1.65 ± 0.06	1.59 ± 0.06
solubility parameters (cal/cm^3)$^{1/2}$	5.76 ± 0.29	6.24 ± 0.23	5.88 ± 0.23

[a] The reference values were from the database of Design Institute for Physical Property Data (DIPPR) Project 801, American Institute of Chemical Engineers (AIChE).
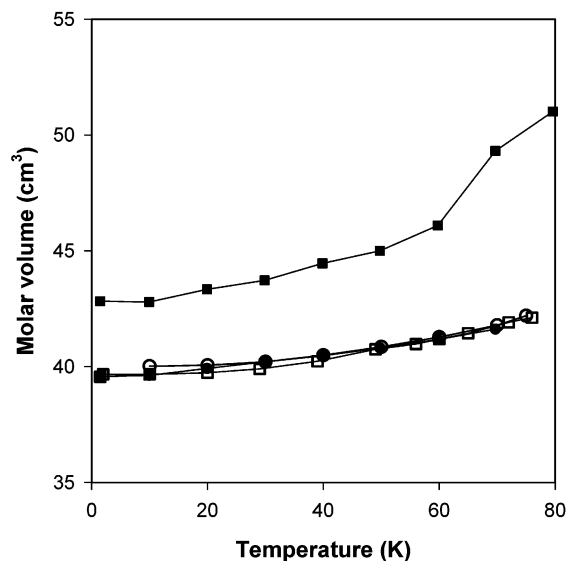

Figure 3. Temperature and volume relation of CF$_4$ crystal under 1 atm: ○, experiment (ref 35); □, experiment (ref 18); ●, simulation using new F parameter set with $\zeta = 15$ in Table 3; ■, simulation using the old F parameter set (ref 9).

3.3825, $\zeta = 15$) in Table 3, and the results from the two independent experimental studies[18,35] were achieved. These values are to similar to $D_{vdW} = 0.0735$ kcal/mol ($\epsilon = 37$ K) and $R_{vdW} = 3.311$ Å ($\sigma = 2.95$ Å) as determined by Nose and Klein[8], $D_{vdW} = 0.0795$ kcal/mol ($\epsilon = 40$ K), $R_{vdW} = 3.339$ Å ($\sigma = 2.975$ Å) as reported by Mezei et al.,[36] and $D_{vdW} = 0.0424$ kcal/mol, $R_{vdW} = 3.395$ Å, $\zeta = 15.432$ as reported by Byutner et al.[37]

We tested the transferability of the $\zeta = 15$ fluorine parameter set to other perfluoroalkane compounds. We calculated the solubility parameter of simple perfluoroalkane compounds such as C_2F_4, C_3F_8, and C_4F_{10}. Of course, a systematic way to assign atomic charges and an accurate dihedral potential are both needed for property estimations in these compounds. For the sake of the discussion flow, we defer the presentation of these two important issues to sections 2.3 and 2.4, respectively.

The solubility parameter is defined by[38,39]

$$\delta = \left(-\frac{U_m}{V_m} \right)^{0.5} = \left(\frac{\Delta H_{vap} - RT}{V_m} \right)^{0.5} \quad (4)$$

where U_m/V_m is the cohesive energy density, $-U_m$ is

Table 5. Comparison of Energy-Minimized Conformations between Dreiding Type Force Field and Quantum Mechanics C_6F_{14}

	trans minus		trans plus	
	quantum	force field	quantum	force field
ϕ_1	−165.0	−165.9	165.0	165.9
ϕ_2	−163.2	−163.2	163.2	163.2
ϕ_3	−165.0	−165.9	165.0	165.9

the molar internal energy (the molar potential energy of a material relative to the ideal vapor at the same temperature), and V_m is the molar volume (note that the valence force field, introduced in section 2.4, was used in the calculations involving the $n = 2$, 3, and 4 perfluoroalkanes). In Table 4, it is clear that the new fluorine van der Waals parameter set is adequate to describe the condensed phase densities and heats of vaporization of liquid perfluoroalkanes. Table 4 also illustrates the effect of using the two most widely employed atomic partial charge assignment methods. Ten simulated samples were used to obtain an estimate of the precision of the calculated solubilities and densities. Although both sets of charges overestimate the solubility parameter, electrostatic potential charges predict the correct solubility parameter and densities within the experimental error.

2.3. Atomic Charges. B3LYP geometry optimizations were carried out in perfluorohexane using the 6-31G* basis set. Constrained dihedral angles ($\phi_1 = \phi_2 = \phi_3$; see Table 5) from $\phi = 150°$ to $\phi = 180°$ in increments of 2° were employed, while all other coordinates were allowed to relax. Mulliken population atomic point charges (MUL) and electrostatic potential (ESP) were calculated at each of the optimized geometries. We refer to these as polarized charges. Mulliken population charges are usually preferred since their values are conformationally less sensitive than ESP charges, allowing for a less ambiguous energy breakdown. For this reason, in discussions of conformational energetics, we prefer to use Mulliken charges. Neither method provides a good description of electrostatics when point charges are insufficient to represent the full charge distribution of the molecule, in particular when high symmetry is present. Such is the case of perfluorinated ethane and perfluorinated benzene. For the
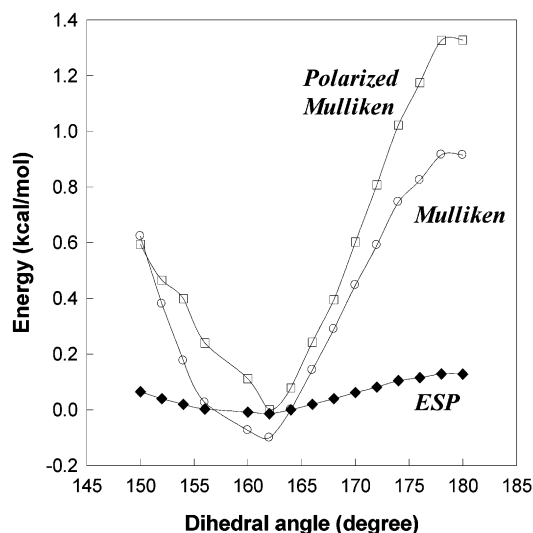
Figure 4. Comparison of classical electrostatic energies for perfluorohexane conformations vs charge assignment method. Polarized are Mulliken population charges from the quantum-optimized geometries. Fixed electrostatic potential (ESP) and Mulliken (MUL) charges are from the minimum energy conformation ($\phi_1 = \phi_2 = \phi_3 = 162°$). A spline curve connects the points as a guide to the eye. Fixed electrostatic potential (ESP) charges (◆), fixed Mulliken population charges (○), and polarized Mulliken charges calculated at each of the conformer's geometries (□) are used.

most part atomic centered point charges are incapable of reproducing the quantum estimated quadrupole moments. ESP charges, however, often perform better for properties where the far field electrostatics is important. Such is the case in the estimation of heats of vaporization, molar volumes and thus solubility parameters (see Table 4). Classical electrostatic energies

$$E_Q = 322.0637 \sum_{i>j} \frac{Q_i Q_j}{\epsilon R_{ij}} \qquad (5)$$

were calculated at the quantum optimized geometries using polarized Mulliken charges as well as fixed Mulliken and ESP charges corresponding to the charges at the minimum conformation, found at $\phi = 163.2°$. $\epsilon = 1$ is the dielectric constant, Q_i and Q_j are the atomic charges in electron units, and R_{ij} is the distance in Å, while 322.0637 converts the electrostatic energy to kcal/mol. As customary the bonded 1−2 and next nearest bonded 1−3 electrostatic interactions are excluded from the sum. The symmetrized fixed atomic partial charges, in electron units, are as follows: Mulliken −0.26 (CF_2 fluorine), +0.52 (CF_2 carbon), −0.24 (CF_3 fluorine), +0.72 (CF_3 carbon); ESP −0.09 (CF_2 fluorine), +0.18 (CF_2 carbon), −0.13 (CF_3 fluorine), and +0.39 (CF_3 carbon). Note that ESP charges are significantly smaller than Mulliken population charges. However, both sets predict a maximum at $\phi = 180°$ and a minimum around $\phi = 162°$ in the electrostatic energies computed at the quantum optimized geometries (Figure 4). Boyd noticed that polarization, due to conformationally dependent atomic charges, increases somewhat the energy of the trans conformation, $\phi_t = 180°$. Nonetheless, the overall shape of the polarized Coulomb potential reflects closely that of the electrostatics with fixed Mulliken charges.

Because fixed charges are most useful in molecular dynamics calculations, we prefer them to polarized charges. We use Mulliken charges whenever conforma-

Table 6. Dreiding Type Valence Force Field and Fourier Multicomponent Torsion for Perfluoroalkane Molecules

(a) Dreiding Type Valence Force Field					
bond stretching	$E_r = {}^1\!/_2 K_r (R - R_0)^2$				
valence angle bending	$E_\theta = {}^1\!/_2 [K_\theta / \sin^2 \theta_0](\cos\theta - \cos\theta_0)^2$				
dihedral angle torsion	$E_\phi = {}^1\!/_2 V(1 - d \cos 3\phi)$				
E_r	C−C	K_r	429.320	R_0	1.498
	C−F		605.260		1.336
E_θ	C−C−C	K_θ	106.274	θ_0	122.554
	F−C−C		100.337		118.320
	F−C−F		108.240		121.502
E_ϕ	C−C−C−C	V	6.434	d	1
	F−C−C−C		8.244		1
	F−C−C−F		8.085		−1

(b) Fourier Multicomponent Torsion					
dihedral angle torsion		$E_\phi = {}^1\!/_2 \sum_{n=1}^{m} V_n (1 - d_n \cos n\phi)$			
E_ϕ	C−C−C−C	V_1	86.4305	d_1	1
		V_2	9.2812	d_2	1
		V_3	18.2580	d_3	1
		V_4	9.8535	d_4	1
		V_5	9.7520	d_5	1
		V_6	0.8151	d_6	−1
	F−C−C−C	V_3	2.0000	d_3	−1
	F−C−C−F	V_3	2.0000	d_3	−1

tional issues of isolated gas-phase molecules are discussed because the far field electrostatics is not relevant in such situations. We recommend the use of electrostatic potential derived charges (ESP) for estimation of condensed phase properties.

2.4. Dihedral Force Field. One may adopt the view that dihedral potentials are whatever energetics are left once all other valence and nonbond energetics are fully accounted for, the nature of a dihedral potential arguably not being as fundamental as electrostatics or van der Waals interactions. In such cases, a simple dihedral potential may be employed near the bottom of the most stable conformation to fit such energetics and vibrational frequencies. On the other hand, conformational stability over a broad range of conformations can be arbitrarily imposed by choosing as complex a form for the dihedral potential as needed to fit all the stable conformational states of the molecule as well as the energy barriers between them. The main purpose of the present work is to assign the internal energy inasmuch an unambiguous form as possible, particularly for the helical to all-trans conformational transition in linear perfluoroalkanes. Consequently, we accommodate both views and show that both lead to the same conclusion regarding the origin of helicity. Thus, for the dihedral potential we present two separate approaches: (1) a simple one-term dihedral potential, within the level of the Dreiding force field, and (2) a multicomponent periodic dihedral potential.

On the basis of the newly developed nonbond fluorocarbon parameter set presented here, the valence force field for perfluoroalkane compounds was completed using the HBSVD method as shown in Table 6. For simplicity the cross terms employed in the valence force field for CF_4 were not used here. The one term Dreiding dihedral potential in Table 6a is what one might need for fitting the vibrational torsional frequency of a simple molecule such as perfluorinated ethane. The multicomponent ($m = 6$) dihedral backbone (C−C−C−C) potential function is what is require in order to fit the full range of conformational energetics (minima and barriers). The parameters in the multicomponent dihedral
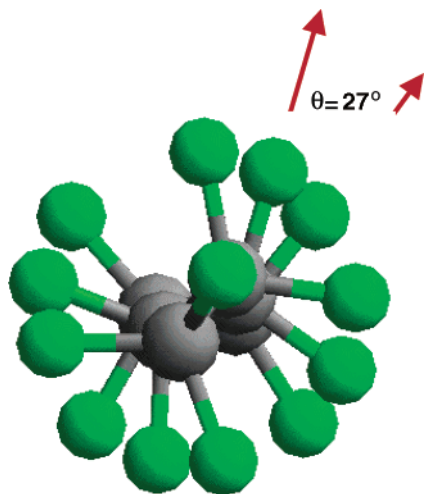
Figure 5. DFT quantum optimized structure of perfluorohexane with a 6-31G* basis set and B3LYP exchange-correlation functional. The helical C−C−C−C twist angle of 16.8° corresponds to a dihedral angle of $\phi = 163.2°$ and to a projected 1−5 F···F angle of $\phi = 27°$.

potential were fitted to reproduce the quantum energetics of C_4F_{10} presented in section 3.1.

3. Conformational Analysis

3.1. C_4F_{10} and C_6F_{14}. By combining the valence force field, shown in Tables 6 a and 6 b, with the new F parameter set ($R_{vdw} = 3.3825$, $D_{vdW} = 0.05092$, and $\zeta = 15$), and fixed Mulliken charges, the helical conformations of C_6F_{14} were investigated. The quantum optimized geometry for perfluorohexane is shown in Figure 5.

Full quantum geometry optimizations for perfluorinated hexane gave a helical twist angle of 16° for the three central dihedral bonds, in good agreement with the experimental value of 14° in poly(tetrafluoroethylene). Table 5 shows good agreement between the quantum mechanically optimized conformation of perfluorohexane and predictions from Dreiding type force field with simple torsion functions. Note that the dihedral potential is a simple one-term potential (Table 6a), with minima at 0 and 120° and maxima at 60 and 180°. Nonetheless the correct t_+ and t_- minima are both correctly predicted without any additional refitting of the force field. Figure 6 gives a summary of the relative energy values for the individual terms in perfluorobutane using the multicomponent force field in Table 6b. For the case of constraint minimization, six stable minima are identified in the current force field: $t_+ = 164$, $g_+ = 95$, and $h_+ = 60$, and their mirror image enantiomeric conformations $t_- = -164$, $g_- = -95$, and $h_- = -60$. Notice the apparent large Coulombic energy barrier at 0°, twice as large as the quantum barrier. This is due to the use of fixed electrostatic charges. The net force field barrier is brought in compliance with the quantum value by the multicomponent dihedral potential.

Figure 7 shows the relative force field energy values, $E = E(\phi) - E(\phi_{t_+})$, near the optimum helical geometry for C_4F_{10} ranging from 150 to 180°, and a comparison with quantum energies (solid circles). Note that only the electrostatic component shows a minimum near the quantum predicted equilibrium dihedral angle ($\phi = 164°$). The electrostatic energy barrier using fixed Mulliken charges matches closely the quantum calcu-
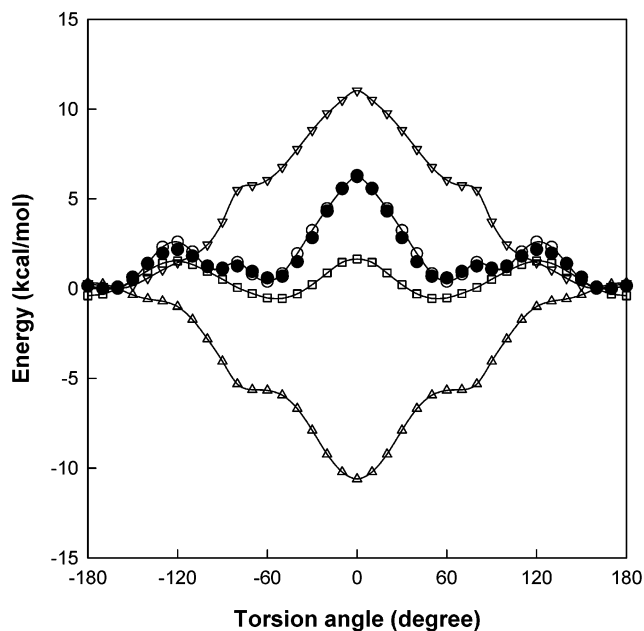

Figure 6. Summary of the relevant force field energy terms for perfluorinated butane as a function of dihedral angle. Plot shows relative energy values in kcal/mol. The zero of energy has been set to the lowest energy conformer ($\phi = 164°$). Geometries are minimized with the C−C−C−C dihedral angle constrained to the value of ϕ depicted in the x axis. Energy components are total force field energy (○), van der Waals (□), electrostatics (▽), torsion (△), and quantum energy (●).
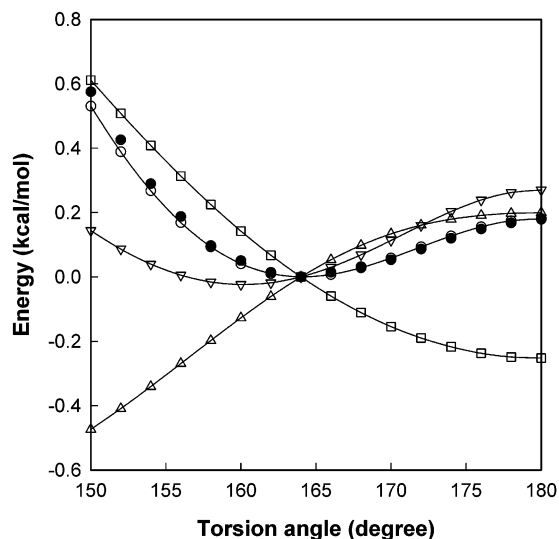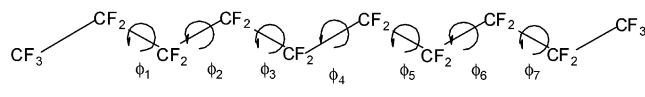

Figure 7. Relative energy components near the equilibrium dihedral angle for perfluorobutane. The zero of energy for each energy component has been set to the component's value in the lowest energy conformer ($\phi = 164°$): ●, quantum energy; ○, total force field energy; △, torsion; □, van der Waals; ▽, electrostatic.

lated energy barrier at $\phi = 180°$. The van der Waals component shows a minimum, -0.2 kcal/mol, at the all-trans $\phi = 180°$ conformation. The dihedral potential shows a barrier of $+0.3$ kcal/mol with respect to the ϕ_{t_+} state in the all-trans conformation.

3.2. $C_{10}F_{22}$ and $C_{20}F_{42}$. Full molecular mechanics minimizations of longer perfluorinated alkanes ($C_{10}F_{22}$ and $C_{20}F_{42}$) were conducted. The t_+, t_-, h_+, and h_- conformations remain unchanged within a few degrees when starting form the nominal dihedral angle values. However, the g_+ and g_- states are unstable. Full

Table 7. Comparison of Energy-Minimized Conformations between Dreiding Type Force Field and Quantum Mechanics for $C_{10}F_{22}$[a]

	g_+		h_+		t_+	
	quantum	force field	quantum	force field	quantum	force field
ϕ_1	165.5	163.4	58.1	61.8	163.2	165.9
ϕ_2	54.6	59.1	58.7	59.8	163.2	163.5
ϕ_3	164.4	160.6	58.0	59.9	163.2	163.6
ϕ_4	54.6	58.7	58.2	60.0	163.2	163.7
ϕ_5	164.4	160.6	58.2	59.9	163.2	163.6
ϕ_6	54.6	59.1	58.3	59.8	163.2	163.5
ϕ_7	165.5	163.4	57.9	61.8	163.2	165.9

[a] Conformations are labeled with the nominal starting angles prior to minimization.

Table 8. Unit Cell Parameters, Experimental vs Predicted, for the M Form of $C_{20}F_{42}$[a]

unit cell parameter	experiment[43]	force field minimization	75 K *NPT* molecular dynamics
A, Å	9.65	9.86	9.67
B, Å	5.70	5.39	5.52
C, Å	28.3	27.9	28.03
α, deg	90	90	89.6
β, deg	97.2	97.0	95.4
γ, deg	90	90	84.6
density, g/cm³	2.232	2.339	2.312
av dihedral angle, deg	N/A	166.6	172.3
helix *z* per CF_2, Å	1.415[b]	1.395	1.401

[a] Results are from the Dreiding type force field using the simple torsion potential. Minimization within *Pc* space group; molecular dynamics with reduced *P*1 symmetry   [b] Estimated from *C* axis length.

minimization leads to torsional angles alternating between 60 and 160° (−60 and −160°) throughout the backbone for the g_+ (g_-) conformation. This was confirmed with quantum mechanical calculations. Table 7 shows comparison between quantum mechanics and force field predictions. No symmetry was applied in the quantum calculations. The agreement is good. Figure 8 depicts all six stable conformations for $C_{20}F_{42}$.

Without further adjustments in the force field, we predict the low temperature (monoclinic) form of perfluoro-*n*-eicosane ($C_{20}F_{42}$). The crystal structure of $C_{20}F_{42}$ is composed of stacking layers. Within each layer, the molecules form a two-dimensional lattice. The molecular crystal usually passes through several solid phase transitions before melting. The first order phase transitions are mainly due to disorder in rotational motions within each molecule or translational motion among molecules.[40−43] Perfluoro-*n*-eicosane has three solid phases, namely, M (monoclinic) for *T* < 146 K, I (intermediate) for 146 < *T* < 200 K, and R (rhombohedral) for *T* > 200 K.[43] The unit cell of the M phase of $C_{20}F_{42}$ consists of two molecules. One is left-handed, and

the other is right-handed. After energy minimization, using the force field introduced here, molecular mechanics predict the cell parameters listed in Table 8. The values are all in good agreement with experimental results. Figure 9 shows the helical geometry of the M form upon minimization and the packing in the $C_{20}F_{42}$ unit cell. The atomic coordinates have not been experimentally determined for the solid. However, the X-ray diffraction pattern for monolayer[11] is available for comparison purposes. Figure 10 shows the X-ray diffraction pattern, using the X-ray diffraction module in Accelerys' Cerius² package, calculated from an MD simulation on the $C_{20}F_{42}$ crystal at 300 K for 100 ps. This X-ray diffraction pattern is in good agreement with the aforementioned room-temperature experimental observations.[11] Table 9 contains predicted mechanical properties of perfluoro-*n*-eicosane estimated with the current force field using the second derivative method (low-temperature limit). Experimental measurements at low temperature are not available for comparison. The speed of sound was calculated from the elastic stiffness matrix and the calculated density. The self-assembly and thermal transitions of perfluoroeicosane
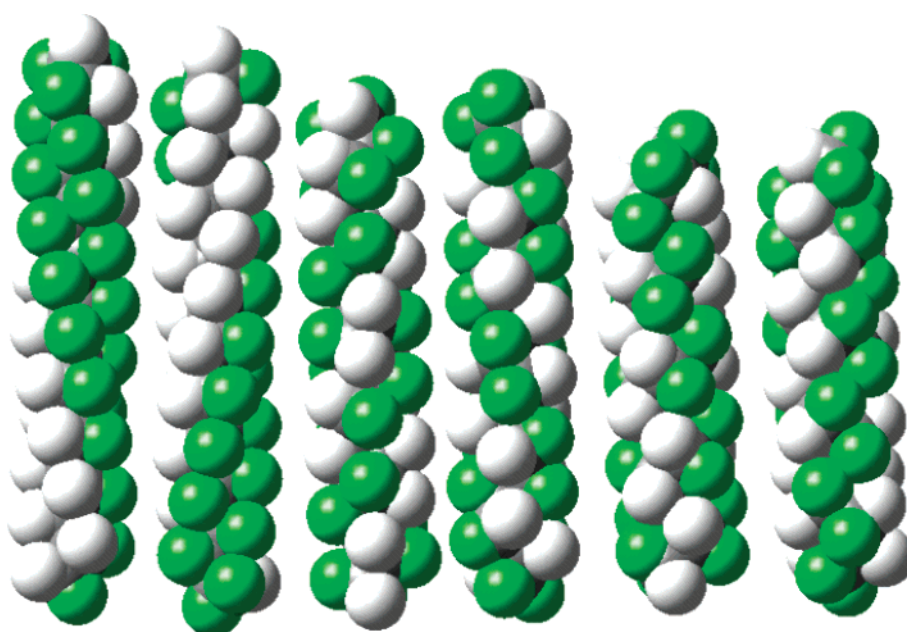

Figure 8. Predicted stable helical conformations for $C_{20}F_{42}$. From left to right t_+, t_-, g_+, g_-, h_+, and h_- enantiomeric pair conformations. The atoms are colored to facilitate the viewing of their helical nature. The tighter the dihedral angle (from 164 to 60°) the shorter the molecule gets. Fluorine atoms of each color would be located on the same side if the molecule were prepared in the all-trans conformation.
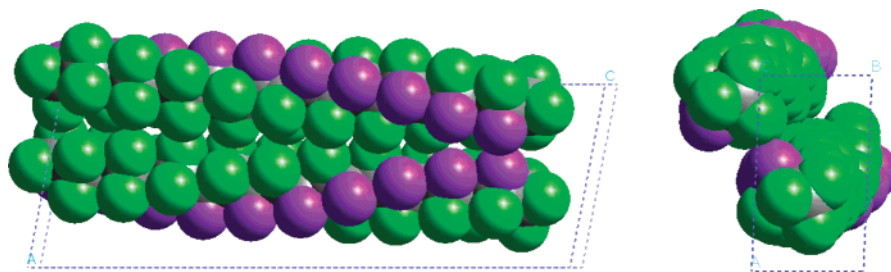
Figure 9. Simulated monoclinic (M phase) structure of $C_{20}F_{42}$, looking through the crystal along the C direction on the left and along the B direction on the right. ($A = 9.65$ Å; $B = 5.70$ Å; $C = 28.3$ Å, $\beta = 97.2°$; $\alpha = \gamma = 90°$.)
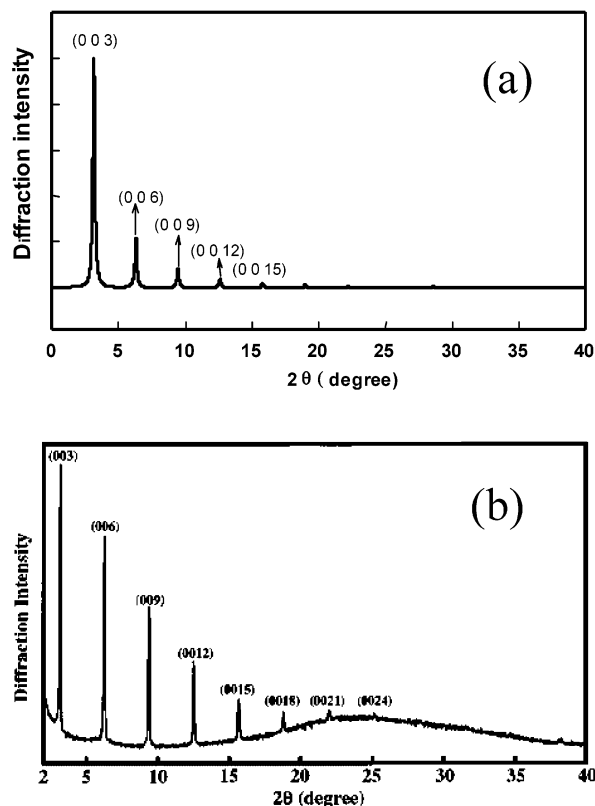

Figure 10. (a) Calculated vs experimental (b) X-ray diffraction for vapor-deposited $C_{20}F_{42}$ epitaxially grown monolayer on a hydrophobically pretreated glass slide.[11] Intensity units are arbitrary. Experimental data is shown without baseline adjustments. Reprinted from ref 11. Copyright 1999 American Chemical Society.

($C_{20}F_{42}$) will be compared to experimental results in a separate publication.[12]

4. Discussion

Perfluorinated alkanes have significant technological uses in various areas of chemistry and material science. It is of great importance to develop models that are capable of providing a deeper understanding of the unusual properties of these materials, particularly relevant structural features. We have presented a detailed breakdown of the energetics involved in the conformations of perfluorinated *n*-alkanes. Independent parameter determinations for van der Waals, electrostatics, and dihedral potentials were conducted through a combination of experimental and ab initio data. Thus, van der Waals interactions were obtained from thermodynamic properties of tetrafluoromethane and validated against other low molecular weight perfluorinated *n*-alkanes; dihedral potentials were optimized through a biased Hessian vibrational frequency analysis as well

Table 9. Mechanical Properties of the Low-Temperature Monoclinic Form of $C_{20}F_{42}$ Calculated Using the Second Derivative Method[17] and the Dreiding Type Force Field in Table 6a

Elastic Stiffness Constants C_{ij} ($\sigma_1 = C_{ii}*\epsilon_i$)					
12.4176	3.6914	2.9834	0.0265		
3.6914	9.1955	3.1303			0.6635
2.9834	3.1303	30.6235	0.8523	3.2261	
0.0265		0.8523	1.5190		0.6988
		3.2261		1.5877	0.3324
	0.6635		0.6988	0.3324	0.087
Elastic Compliance Constants S_{ii} (1/GPa) ($\epsilon_i = S_{ii}*\sigma_i$)					
0.115			0.026	0.168	
	0.099	0.009			0.230
	0.009	0.038	0.046		
0.026		0.046	0.142		1.010
0.168				0.778	0.686
	0.230		1.010	0.686	

bulk module	6.610
compressibility	0.151
isotropic Lame constants	
λ	15.282
μ	1.064

axes of the Young moduli		Poisson ratio			
X	8.66	E_{xy}	0.294	E_{xz}	0.230
Y	10.040	E_{yx}	0.341	E_{yz}	
Z	26.010	E_{zx}	0.69	E_{zy}	

Velocities of Sound					
X_1	0.076	X_2	0.782	X_3	2.315
Y_1	0.326	Y_2	0.874	Y_3	1.980
Z_1	0.707	Z_2	0.810	Z_3	3.626

as the full range of stable conformations of perfluorinated *n*-hexane, and electrostatic terms were determined from quantum mechanical calculations of point charges. We further validate the current force field by predicting the monoclinic structure of perfluoroeicosane ($C_{20}F_{42}$) and its low-temperature mechanical compliance matrix. The force field is transferable and provides good to excellent agreement in the vibrational frequencies and PV data for CF_4, densities and solubility parameters (heats of vaporization and densities) of low molecular weight perfluoroalkanes, and the X-ray structure of $C_{20}F_{42}$. Contrary to previous studies we find that 1−5 van der Waals interactions favor the all-trans conformation although the new potential is more repulsive than others used in similar studies.[6,7]

An analysis of 1−5 nonbond interactions for a short segment of a quantum geometry optimized perfluorinated *n*-alkane is shown in Figure 11. Pertinent distances for the all-trans and helical conformations of the central segment in C_6F_{14} are shown. Table 10 summarizes the change in the van der Waals and electrostatic energies when transforming from the all-trans to the helical conformation. The van der Waals term is positive for the force field presented in this work but
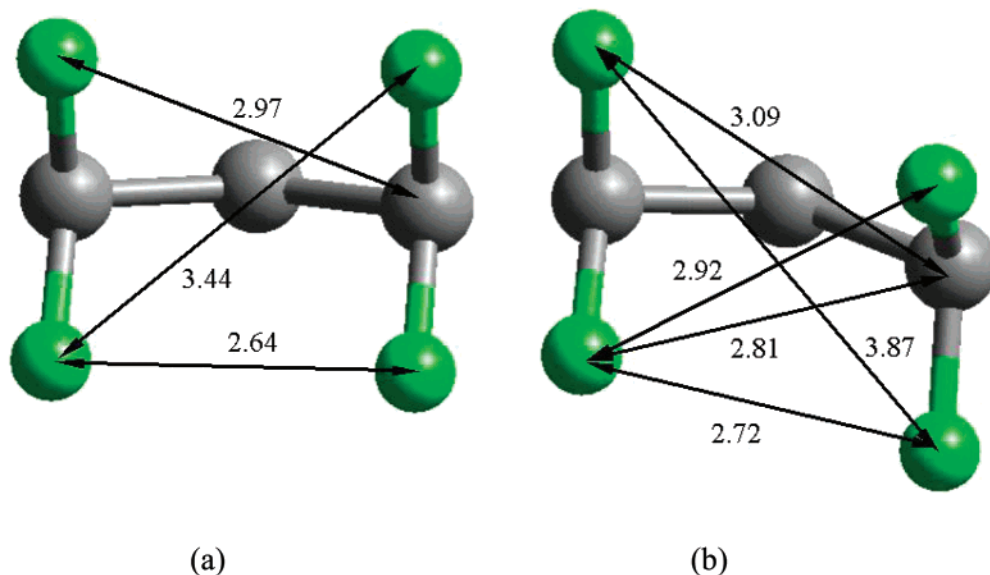
(a)   (b)

Figure 11. Relevant 1−5 fluorine−fluorine and 1−4 fluorine−carbon van der Waals distances in the all-trans (a) and the helical (b) conformations of perfluorohexane. Distances are from the C_6F_{14} quantum-mechanical-optimized geometry.

Table 10. Breakdown of the Energy Differences between the Helical and the All-Trans Conformations of C_6F_{14}, $\Delta E_{helical-trans}$ in kcal/mol, Using the Quantum Mechanical Mulliken Population Charges and Optimized Geometries

E(helical) − E(trans) nonbond terms	this work	ref 8
van der Waals	0.71	−1.20
electrostatics	−0.91	N/A
total nonbond	−0.21	−1.20

components pairwise	van der Waals				electrostatics			tot. nonbond
	all pairs	1−4	1−5 to 1−8		all pairs	1−4	1−5 to 1−8	
F−F	−0.22	0.73	−0.95	24	1.21	0.75	0.46	0.99
C−C	0.00	0.00	0.00		1.28	−0.03	1.31	1.28
C−F	0.93	0.96	−0.03		−3.41	−0.95	−2.46	−2.47
tot.	0.71	1.69	−0.98		−0.91	−0.23	−0.69	−0.21

negative for the Nose−Klein vdW parameters.[6−8] Notice that the electrostatic interaction stabilizes (negative value) the helical conformation in the present work. These remaining results provide additional support to classical electrostatics as the source of helicity in perfluorinated *n*-alkanes.

Figure 12 shows that the helical to trans transformation energies, calculated from quantum mechanics (B3LYP, 6-31G*), vs carbon number ($n = 6−14$) more closely resemble the long-range electrostatics than the short-range van der Waals interactions. Van der Waals terms, parameters systematically determined from the thermodynamic properties of low molecular weight fluorocarbons, favor the all-trans conformation (Figure 7). Consequently, van der Waals interactions cannot be the source of helicity in these compounds. Table 10 shows a detailed breakdown of the helical to all-trans conformational transformation for C_6F_{14}. The C−F electrostatic component is most responsible for the stability of the helical conformation. Reference 8 force field and this work show that the 1−5 F−F interactions also add stability.

It can be argued that perfluorinated hydrocarbon helicity is not preserved in the condensed phase, washed out by the molecular packing energy fluctuations. Molecular dynamics force field calculations depicted in Figure 13 shows that the helical conformations are stable in the condensed phase over a significant range of temperatures, giving rise to bimodal (chiral) dihedral distributions (t_+ and t_- states). At higher temperatures

the conformations become trans on average but broadly populated at t_+ and t_- states. Figure 14 illustrates the chiral conversion of perfluorinated eicosane over the range of temperatures for which thermodynamic transitions have been observed. Note that the chiral order−disorder transitions predicted from molecular dynamics calculations using the force field presented in this work are consistent with the experimental results of Schwickert et al.[43]

It is always possible to find a set of van der Waals parameters that reproduce the helical nature of linear fluorocarbons and give reasonable predictions for the thermodynamic properties of pure fluorocarbons,[44] in the absence of electrostatics (no partial charges). However, because electrostatics are ignored, such force field cannot properly describe the physical interactions between fluorocarbons and polar compounds. We aimed in this paper to develop a full physical, transferable force field for linear perfluorocarbons, capable of explaining the source of helicity in these compounds. Our results show that electrostatic interactions stabilize the helical conformations of linear perfluorinated alkanes.

5. Conclusions

We conclude from the quantum and force field energetics presented here that the origin of helicity in perfluorinated *n*-alkanes is the electrostatic repulsion between fluorine atoms. A fixed set of Mulliken population charges, determined from quantum mechanical
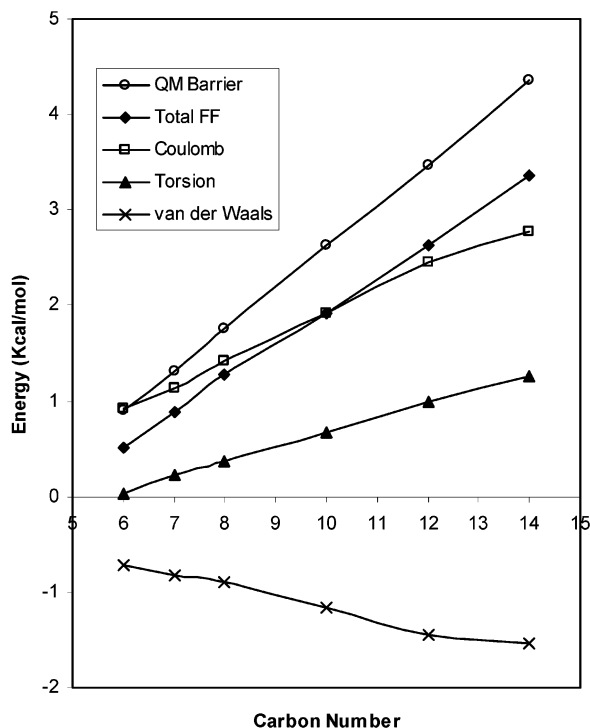
Figure 12. Energy components for helical to all-trans conformation transformation of perfluorinated *n*-alkanes as a function of carbon number. For $n > 6$ each CF_2 adds ca. 0.4 kcal/mol to the overall conversion energy. Geometries were quantum mechanically fully optimized for the helical conformations. Constraints ($\phi = 180°$) of nonterminal dihedral angles were used for the all-trans geometry optimizations. Fixed quantum Mulliken charges, calculated at the helical conformation, were used throughout. Angle bends and bond stretch contributions are not depicted.
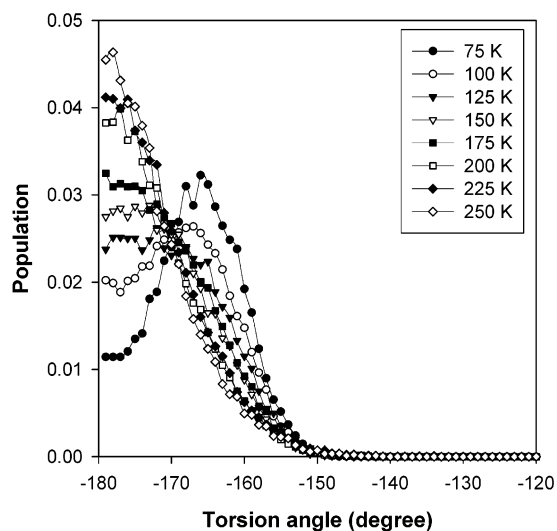
Figure 13. Temperature dependence of of the torsion angle (C−C−C−C) in perfluorinated eicosane.

calculations, predicts the correct position of the minima within 2°, and other than a constant shift factor of less than 1 kcal/mol, the transformation energy between helical and all-trans conformations for a series of perfluorinated *n*-alkanes ($n = 6$−14). A simple, one Fourier term, dihedral potential (obtained from a frequency mode analysis at the minimum energy geometry) destabilizes the all-trans conformation. However, by itself it predicts the incorrect helical angle (120 vs 164°). The full force field, which includes electrostatics, presented here predicts the correct quantum determined
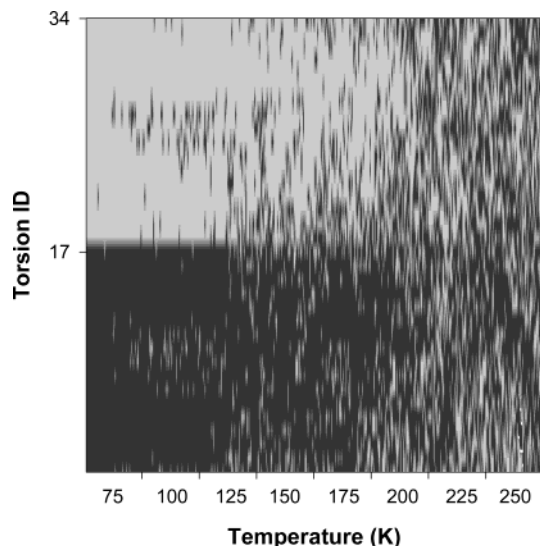

Figure 14. Temperature evolution of the backbone dihedrals in the $C_{20}F_{42}$ two molecule unit cell. Dihedral angles for the low-temperature right (left) handed helical molecule are labeled 1−17 (18−34). Black indicates a 1-dihedral state while white indicates a 1+ state. Both molecules exist in a pure helical state (t_+ or all t_-) below 140 K, in a mixture of states between 140 and 200 K, and in a nonchiral state above 200 K in agreement with experimental observations.

helical angles to within 0.1°. Favorable electrostatic attractions between the carbon and fluorine 1−5 atom pairs are most responsible for the added stability of the helical conformation. Understanding the origin of helicity, in this important class of polymers, points the way toward understanding the structure and conformations of other non-hydrogen bond containing polymers and perhaps to the development of new polymers with helical chiral structures. In addition, the systematic determination of force field parameters, including van der Waals, may aid the understanding of the physical properties of condensed phase and self-assembled monolayers prepared with this important class of commercial polymers.

References and Notes

(1) Bunn, C. W.; Howells, E. R. *Nature (London)* **1954**, *174*, 549.
(2) Albinsson, B.; Michl, J. *J. Am. Chem. Soc.* **1995**, *117*, 6378.
(3) Boyd, R. H.; Kesner, L. *J. Chem. Phys.* **1980**, *72*, 2179.
(4) Dixon, D. A. *J. Phys. Chem.* **1992**, *96*, 3698.
(5) Smith, G. D.; Jaffe, R. L.; Yoon, D. Y. *Macromolecules* **1994**, *27*, 3166.
(6) Rothlisberger, U.; Laasonen, K.; Klein, M. L.; Sprik, M. *J. Chem. Phys.* **1996**, *104*, 3692.
(7) Sprik, M.; Rothlisberger, U.; Klein, M. L. *Mol. Phys.* **1999**, *97*, 355.
(8) Nose, S.; Klein, M. L. *J. Chem. Phys.* **1983**, *78*, 6928.
(9) Karasawa, N.; Goddard, W. A., III. *Macromolecules* **1992**, *25*, 7268.
(10) Karasawa, N.; Goddard, W. A., III. *Macromolecules* **1995**, *28*, 6765.
(11) Nishino, T.; Meguro, M.; Nakamae, K.; Matsushita, M.; Ueda, Y. *Langmuir* **1999**, *15*, 4321.
(12) Zhou, Y.; Caldwell, G.; Che, J.; Cagin, T.; Blanco, M.; Ross, R. B.; Goddard, W. A. Manuscript in preparation.

(13) Dasgupta, S.; Goddard, W. A., III. *J. Chem. Phys.* **1989**, *90*, 7207.

(14) Dasgupta, S.; Yamasaki, T.; Goddard, W. A., III. *J. Chem. Phys.* **1996**, *104*, 2898.

(15) Wang, X. G.; Sibert, E. L.; Martin, J. M. L. *J. Chem. Phys.* **2000**, *112*, 1353.

(16) Mayo, S. L.; Olafson, B. D.; Goddard, W. A., III. *J. Phys. Chem.* **1990**, *94*, 8897.

(17) Karasawa, N.; Dasgupta, S.; Goddard, W. A., III. *J. Phys. Chem.* **1991**, *95*, 2260.

(18) Fitch, A. N.; Cockcroft, J. K. *Z. Kristallogr.* **1993**, *203*, 29.

(19) Eucken, A.; Schroeder, E. *J. Phys. Chem.* **1938**, *41*, 1B, 307.

(20) Bondi, A. *J. Chem. Eng. Data* **1963**, *8*, 371.

(21) Verlet, L. *Phys. Rev.* **1967**, *159*, 98.

(22) Karasawa, N.; Goddard, W. A., III. *J. Phys. Chem.* **1989**, *93*, 7320.

(23) Nose, S. *Mol. Phys.* **1984**, *52*, 255.

(24) Nose, S. *J. Chem. Phys.* **1984**, *81*, 511.

(25) Hoover, W. G. *Phys. Rev. A* **1985**, *31*, 1695.

(26) Nose, S. *Mol. Phys.* **1986**, *57*, 187.

(27) Parrinello, M.; Rahman, A. *Phys. Rev. Lett.* **1980**, *45*, 1196.

(28) Parrinello, M.; Rahman, A. *J. Appl. Phys.* **1981**, *52*, 7182.

(29) Parrinello, M.; Rahman, A. *J. Chem. Phys.* **1982**, *76*, 2662.

(30) Stephenson, R. M.; Malanowski, S. *Handbook of the Thermodynamics of Organic Compounds*; Elsevier: New York, 1987.

(31) Stewart, J. W.; Rock, R. I. L. *J. Chem. Phys.* **1958**, *28*, 425.

(32) Bohmer, R.; Loidl, A. *J. Mol. Liq.* **1991**, *49*, 95.

(33) Murnaghan, F. D. *Am. J. Math.* **1937**, *49*, 235.

(34) Birch, F. *Phys. Rev.* **1947**, *71*, 809.

(35) Bol'Shutkin, D. N.; Gasan, V. M.; Prokhvatilov, A. I.; Erenburg, A. I. *Acta Crystallogr.* **1972**, *B28*, 3542.

(36) Jedlovszky, P.; Mezei, M. *J. Chem. Phys.* **1999**, *110*, 2991.

(37) Byutner, O. G.; Smith, G. D. *Macromolecules* **2000**, *33*, 4264.

(38) Lide, D. R. *CRC Handbook of Chemistry and Physics*, 80th ed.; CRC Press: Boca Raton, FL, 1999−2000.

(39) Brandrup, J.; Immergut, E. H. *Polymer Handbook*, 3rd ed.; John Wiley & Sons: New York, 1989.

(40) Piesczek, W.; Strobl, G.; Malzahn, K. *Acta Crystallogr.* **1974**, *B30*, 1278.

(41) Strobl, G.; Ewen, B.; Fisher, E. W.; Piesczek, W. *J. Chem. Phys.* **1974**, *61*, 5259.

(42) Ewen, B.; Strobl, G.; Richter, D. *Faraday Discuss.* **1980**, *69*, 19.

(43) Schwickert, H. J.; Strobl, G.; Kimmig, M. *J. Chem. Phys.* **1991**, *95*, 2800.

(44) Borodin, O.; Smith, G. D.; Bedrov, D. *J. Phys. Chem. B* **2002**, *106*, 9912.